A synchrotron x-ray study of a Ti-Si Cf composite during in situ straining

Eric Maire, A. Owen, Jean-Yves Buffière, Philip J Withers

A SYNCHROTRON X-RAY STUDY OF A Ti/SiC_f COMPOSITE DURING IN SITU STRAINING

E. MAIRE[1]*, A. OWEN[2], J.-Y. BUFFIERE[1] and P. J. WITHERS[2]

[1]GEMPPM INSA de LYON, 20 Av. A. Einstein, 69621 Villeurbanne, France and [2]Manchester Materials Science Centre UMIST/University of Manchester, Grosvenor St. Manchester M1 7HS, UK

Abstract—X-ray synchrotron radiography and high spatial resolution strain measurements have been combined to build-up a picture of the micromechanics of the damage that occurs, and the internal stress that causes it, within a Ti/SiC monofilament composite test-piece that was progressively strained in situ on the beam-line. The sample was designed to include a row of fibre ends within the test-piece. The radiographs show that fibre breakages occur during straining, even in the vicinity of the fibre ends. Axial and transverse strain measurements were made along each fibre in the composite as the load was progressively increased using a small X-ray spot size. In the present case interfacial sliding is believed to occur by slipping in or near the 4 μm carbon coating of the SCS-6 fibres. In order to interpret the strain measurements the predictions of a simple axi-symmetric finite element model of the composite are compared with the measured strains.

Keywords: Composites; Fibres; Titanium alloys; Interface; Diffraction

1. INTRODUCTION

The next generation of aeroengines will require new materials that have superior high temperature creep and strength properties relative to those that are used at present. This is because without them it will not be possible to employ innovative integrally bladed ring structures in place of traditional disc assemblies [1]. These structures promise to reduce engine weight drastically, but require new materials to cope with the increased hoop stresses caused by the rotating parts. As a result Ti/SiC monofilamentary composites are of considerable interest technologically.

At the present time relatively little is known about the micromechanics of load transfer between matrix and reinforcement, especially in the region of the fibre ends. Even continuous fibre composites must have some fibre ends, and fibre breakages further increase the number of fibre ends. The effect of fibre ends and breakages have become the focus of concern for composite fabrication. Two factors have held up progress in this area. Firstly it has not been possible to measure the build-up of stress along SiC monofilaments within real metal matrices. This is unfortunate, the measurement of stress/strain along embedded fibres in transparent matrices by Raman strain measurement has provided important insights into the micromechanics [2, 3]. These studies have been instructional from a composite mechanics viewpoint. However, the mechanisms of fibre pull-out are potentially quite different in the present case because of the opportunity for matrix shearing as well as scope for frictional sliding due to the presence of a 4 μm carbon coating on the SCS-6 monofilaments. Secondly, micromechanical predictions of the stress variation have been held up by the lack of reliable critical interfacial shear stress data. This is because, while a number of tests have been developed to evaluate the matrix/reinforcement interface in this system (pull-out [4], push out [5], full fragmentation [6], pull-out/push-back [7], etc), most involve loading geometries quite different from those encountered in practise. As a result the maximum shear stresses derived from each of these methods differ widely.

The European Synchrotron Research Facility has made very intense high energy X-ray beams available for materials research. Using these beams penetrations and data acquisition times are many orders of magnitude greater than can be achieved on lab X-ray sources. This has opened up the possibility of micron resolution X-ray tomography and high spatial resolution (~100 μm probe size) strain measurements, even on materials of relatively high atomic number such as titanium. In this paper we describe the first measurements of strain in individual SiC monofilamentary fibres deep within a titanium alloy matrix.

* To whom all correspondence should be addressed. Tel.: +33-4-72-43-84-99; fax: +33-4-72-43-85-39.

By carrying out tensile tests on a tomographic beam-line (ID19) it has been possible to monitor the accumulation of fibre breakages in a simple test-piece throughout progressive tensile straining. By carrying out similar tensile tests on a high energy diffraction beam-line (ID11) it has been possible to map the distribution of stress between matrix and individual fibres as a function of straining. These results show the classical build-up of stress from the fibre ends and provide important information for the composite modeller.

2. MATERIALS

In order to investigate the role of fibre ends in the build up of stress, a set of idealised composite test-pieces were manufactured. Each test-piece was electro-discharged machined to a plate like geometry (1×10×30 mm) with a narrow region in the centre (1.5 instead of 10 mm wide). In order to study the effect of fibre ends on load transfer, each sample contained a row of fibres that terminated approximately in the centre of the gauge region (Fig. 1). These samples were made from a single foil–fibre–foil ply comprising 100 μm foils of Ti–6Al–4V in which was sandwiched a single row of SCS-6 SiC monofilaments (140 μm diameter, C core with 4 μm C coating). This single ply was cut by guillotine and then placed between two 1mm thick sheets of Ti–6Al–4V so that the fibres terminated between the sheets. This sandwich was then hot pressed at 900°C for 4 h. When electro-discharge machining the samples, great care was exercised to ensure that the fibres were aligned with the tensile axis and the fibre ends formed a row approximately half way along the gauge length (Fig. 1). These test-pieces were then polished to approximately 1 mm total thickness so that they could be tested to failure within the 1.8 kN in situ tensile stage. Two nominally identical samples were studied; sample 1 was examined by X-ray radiography to characterise damage accumulation as a function of applied loading on beam-line ID19 at the ESRF, while the internal strains were mapped in sample 2 as a function of applied load on beam-line ID11.

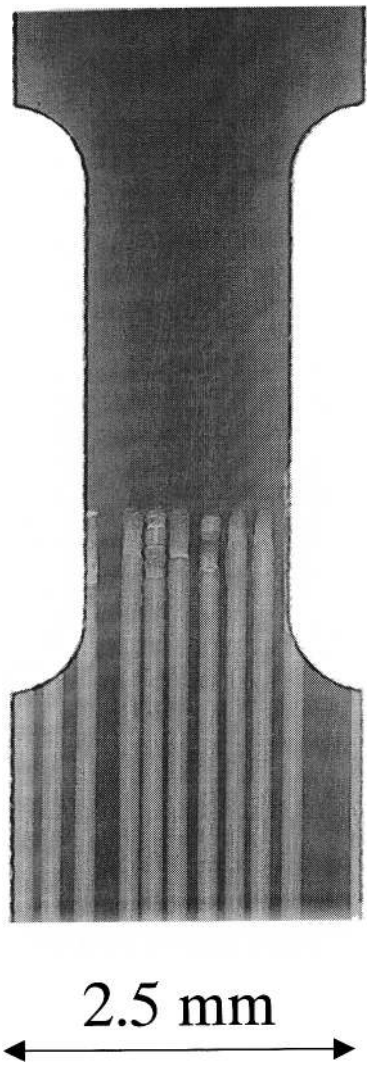

Fig. 1. A simple radiograph showing the tensile test-piece (sample1) and the location of the fibre ends.

3. PART 1. INTERNAL OBSERVATION OF DAMAGE

3.1. Experimental procedure

3.1.1. Imaging set-up. The set-up used for the internal observation of damage during the tensile test on sample 1 is shown in Fig. 2. This part of the experiment was carried out on the tomography beam-line at the ESRF (ID19). The electron beam energy was 6 GeV. The white beam was restricted by slits and monochromated by a set of two parallel silicon single crystals to select photons of 33 keV (for the present application). The unusually large distance of 140 m between the source and the experimental hutch on ID19 lead to a high lateral coherence of the photons. The distance between the sample and the detector (a cooled CCD camera developed at ESRF) was set to about 70 mm. This particularity in the set-up combined with the high lateral coherence of the photons has been shown [8] to lead to an improvement in the detection of phase features (like cracks) due to "phase contrast" which superimposes upon the regular attenuation contrast.

In addition to simple X-ray radiography using single images, the ID19 beam line allows tomographic reconstructions to be performed on structural materials using many images. Tomography is a non-destructive technique which allows the reconstruction of 3D internal structure and damage of a sample [9] with a resolution currently down to 1 μm. For tomography on ID19 the sample is rotated in the beam to provide a set of 900 radiographs which are used by reconstruction software to give a 3D numerical image of the studied material. In the present case of a single layer of fibres, the X-ray observations by

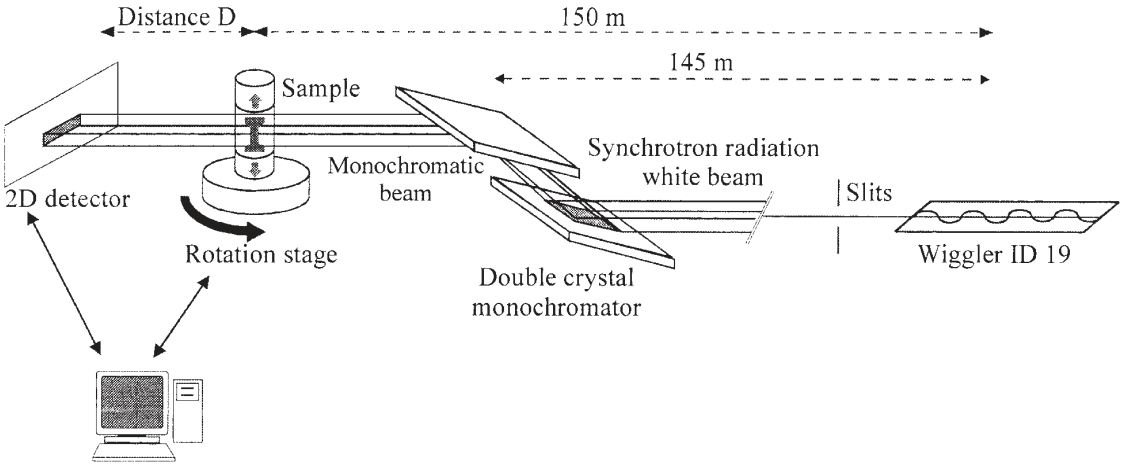

Fig. 2. Set-up used on the ID 19 beam-line at the ESRF to record the radiographs during the in situ tensile test on sample 1.

conventional radiography are relatively easy to interpret. This has the benefit of accelerating the data acquisition from 1–2 h (for a tomograph) to less than a minute (for a single radiograph). Furthermore it reduces the amount of data which must be stored and analysed. For these reasons, radiography was used in preference to tomography for most of the imaging described in this paper. Finally, and in order to compare with simple radiography, a more detailed tomographic inspection has been carried out after the tensile test on sample 2 (the sample used for the strain mapping experiment).

3.1.2. Tensile rig and testing procedure. A tensile rig has been especially designed to allow the observation of damage by tomography during the deformation of materials [9]. This rig can be set on the tomography turntable. In order to avoid obstruction of the sample by the tensile testing rig during the rotation process, the conventional loading posts have been replaced by a PMMA tube which is then used to transmit the load between the upper mobile grip and the lower fixed grip. This tube was carefully polished so as to give negligible attenuation and phase contrast on the 2D radiographs. The force and the cross-head displacement were recorded on a computer and monitored during the test.

A cross-head displacement rate of 150 μm min^{-1} was used for the tests corresponding to an average strain rate of 5 10^{-4} s^{-1}. Once sample 1 was set in the machine, a first radiograph was recorded in order to characterise the initial state. The sample was then loaded step by step in tension: during the test, as the loading was increased the cross-head displacement was interrupted at regular intervals and held constant to facilitate the recording of a radiograph. A slight stress drop, corresponding to a stress relaxation process in the Ti–6Al–4V matrix was recorded when the cross-head displacement was stopped. This effect was largest at the higher loads. In order to avoid blurring caused by displacement of the sample during this relaxation process, the radiographs were recorded when the force on the sample was stabilised.

Sample 1 was oriented normal to the incident beam so that each fibre of the layer could be viewed in transmission by the X-ray camera. The sample was then pulled in the vertical direction along the fibre axis. Seventeen different steps were made during the straining.

3.2. Results

3.2.1. Radiography. Figure 3 shows a set of radiographs illustrating the evolution of the microstructure and damage inside the sample during the test. The corresponding recorded tensile curve is also shown in Fig. 4. Observation of the initial radiograph shows that the internal microstructure of the sample can be reasonably well analysed at this resolution: the carbon cores are clearly visible. Six fibres can be observed in the gauge section of the sample referred to by a number between 1 and 6 as shown in Fig. 3. Due to the action of the guillotine the fibre ends are broken and fibre debris can be observed. In addition, the hot pressing consolidation stage has caused the region near the fibre ends to extrude past the fibres creating holes in the matrix at each end.

On the 2D radiographs, the attenuation contrast given by a crack should be bright because of the local reduction of the X-ray attenuation caused by the cracking. Note however that the breaking events ocurring at the beginning of the test carried out here are delineated by dark lines across the fibres (see for instance fibre 6 in Fig. 3 at step 5). These dark lines are not due to simple attenuation contrast, but to the interference between rays propagating in the cracked fibre and in the adjacent void formed. This phenomenon has been observed previously and generally improves the detection of fine cracks [8, 9]. Therefore, we believe that the cracks are detected at a very early stage when they appear in the fibres despite the fact that the camera resolution is only 6μm. As the

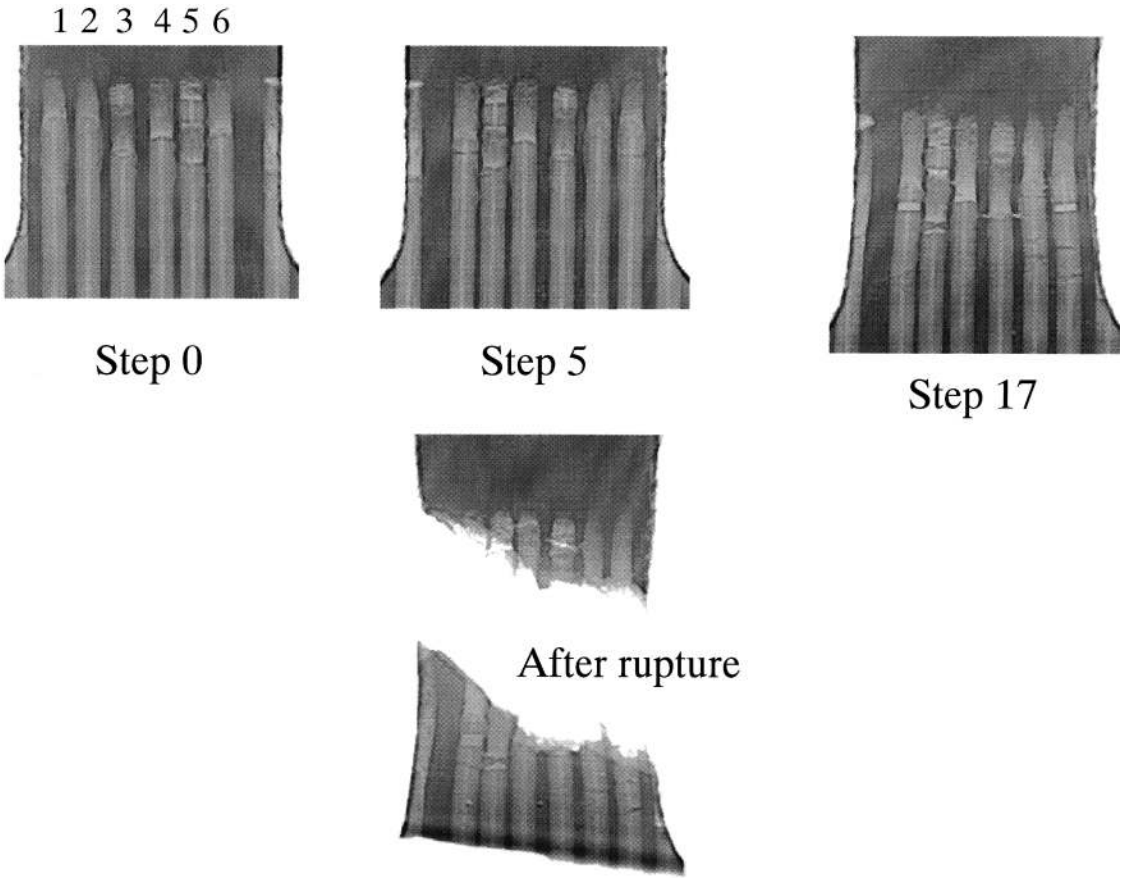

Fig. 3. Sequence of selected radiographs showing the evolution of the microstructure and damage of sample 1 during the tensile test at steps 1 (before the test), 5 (in the elastic regime), 17 (in the plastic regime) and finally after failure.

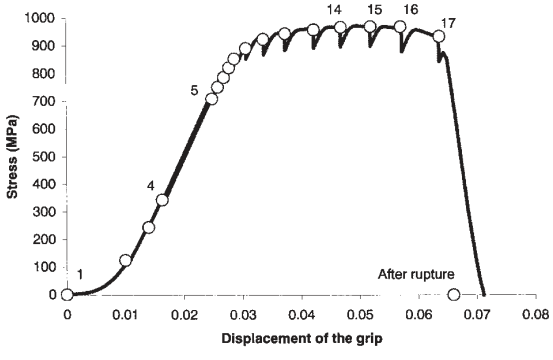

Fig. 4. The tensile stress/strain curve recorded during the radiography experiment on beam-line ID 19.

cracks open wider due to continued straining of the sample, the contrast reverts back to the normal attenuation contrast (the grey level for the cracks gets lighter). Both fibre and matrix cracking/voiding were observed. The detailed observations can be listed as follows. Fibres 1, 2 and 6 cracked less than a few diameters from the fibre ends between steps 4 and 5 (i.e. in the elastic regime). Subsequently, no new breaking events were observed in the first part of the plastic deformation. Fibre 6 broke in two locations between steps 14 and 15 as well as the matrix ligament between fibres 4 and 5 (close to the end of fibre 4). Fibre 5 broke in two locations (possibly because of the influence of the neighbouring crack in fibre 6) between steps 15 and 16 as well as the matrix ligament between fibre 3 and 4. Fibre 5 broke between steps 16 and 17 and thus linked the crack in the matrix with the widely opened crack which originally appeared at the beginning of the test in fibre 6. The cracks observed in the fibres early in the test are due to high axial stresses whereas those observed at the end of the test (between steps 14 and 17) seem to be associated with bending of the fibres in the matrix, due to necking of the sample close to the fibre ends. The final crack formed by linking initial micro-cracks in the fibres and the matrix.

4. PART 2. STRAIN MAPPING

4.1. Experimental set-up and procedure

4.1.1. Set-up. In order to monitor the evolution of internal strains during loading, a similar loading experiment was carried out on sample 2, but with the sample located on the sample stage of the ID11 beam-line. The radiation source for this beam-line is a 24

pole wiggler. These measurements were made in the transmission geometry. A monochromatic beam of 60 keV energy was stopped down by slits to a very small size: 100 μm in the direction transverse to the fibres, and 200 μm in the longitudinal direction of the fibres. The tensile rig described previously was set on an x, z automated translate stage which was used to scan the sample through the incident beam in order to produce 2D strain maps for different tensile loads. The direct beam was stopped by a lead beam stop, and the diffraction rings were recorded on a CCD camera. Seven fibres were identified by scanning the sample transverse to the fibres and observing the appearance and disappearance of the SiC diffraction peaks. With the position of each fibre located, the sample was translated so as to acquire 20 diffraction profiles along the line of each half-fibre (i.e. by translating from positive to negative z in 20 steps). Data acquisition times of a few seconds were used for each profile.

4.1.2. Procedure. A tensile test was performed on sample 2 according to the procedure described in the previous section, but in this case the test was stopped prior to rupture of the sample so that it could also be studied by X-ray tomography on ID19. Seven load steps plus the initial and the final state (after unloading) were characterised by diffraction. The obtained tensile loading curve was quite similar to the one obtained for sample 1 (the maximum difference in stress was less than 5%). The radiograph of sample 2 taken at the end of the tensile test/strain mapping experiment is shown in Fig. 5. The geometry of the scanning beam at the same scale and the pitch of the displacements used for the strain map in the x, z plane is also shown on the figure.

For each tensile loading step, 7×20 diffraction patterns were recorded. As shown in the figure these were along lines including the axes of the fibres in the x direction and with a pitch of 140 μm in the z direction (20 points along the line containing each fibre). There was a slight spatial overlap between each measurement in z (i.e. the pitch was less than the spot size). Note that the measurements in z were made both in the fibres and in the matrix beyond the fibre end (i.e. positive and negative z). In the following analysis, the origin for the z axis was chosen to correspond to the position of the fibre ends (see Fig. 5). The positive values of z correspond to regions within the fibres and the negative values, to regions ahead of the fibres.

4.2. Results

4.2.1. Radiograph of tested specimen. The resolution in the radiograph shown in Fig. 5, recorded on an X-ray film, is 1 μm and the picture was taken in the "phase contrast" conditions so the details of the microstructure are clearly imaged. The sample was radiographed as seen by the beam during the strain mapping exercise. The internal structure seems similar to this observed in sample 1 at the end of the tensile test: seven fibres are visible in the useful part of the sample irregularly spaced in the x direction with debris at the fibre ends, as well as cracks, both widely opened (beginning of the test) like the one visible in fibre 6 and also slightly opened due to the bending of the fibre (end of the test) like the one visible in fibre 1. Fibre 3 was broken in two pieces during the fabrication process as indicated by the intrusion of matrix into the hole during the hot pressing. Note also that fibre 7 is partly cut by the external face of the sample.

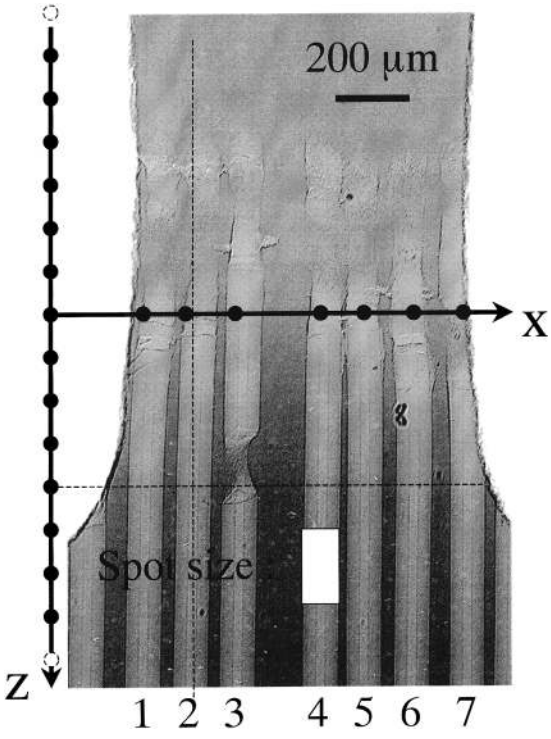

Fig. 5. Final radiograph of sample 2. The actual size of the beam during the diffraction experiment is shown. The dots along the axes indicate the location and spacing between successive diffraction measurements to form a grid.

4.2.2. Strain measurement. The diffraction patterns obtained comprised several rings of different diameters one for each characteristic lattice spacing (hkl reflection). Due to the high degree of anisotropy of the SiC phase, only portions of the rings were visible for the fibres in the polar and equatorial regions, but these portions were sufficient to allow the measurement of the longitudinal and transversal strains. Eight different reflections gave detectable rings on the patterns. The observed peaks have been indexed as presented in Table 1. The α/β Ti–6Al–4V matrix contained a minority cubic phase (5–10% or so) as expected.

The diffraction patterns were first corrected for the distortion of the CCD. In order to deduce the axial and transverse strains, the vertical and horizontal diameters must be measured respectively. The four portions of interest for each ring are thus the vertical

Table 1. Indexing of the peaks observed during the diffraction experiments. The bold columns indicate the three reflections used for the strain measurement

Phase	Ti hex	Ti hex	Ti cub	**Ti hex**	Ti hex	Ti cub	**SiC**	**Ti hex**
hkl indices	100	002	110	**101**	102	200	**110**	**110**
d spacing (Å)	2.54	2.35	2.31	**2.23**	1.72	1.63	**1.54**	**1.46**

and horizontal "cake" segments. To improve counting statistics the ring segments were "caked" to collapse ±12° segments at the two polar and the two equatorial zones to give simple line profiles. The centre of each peak was found by Gaussian peak fitting and by determining the position of the two opposing poles or equatorial zones it was possible to measure the ring diameter D at these positions. By monitoring the variation in diameter ΔD during the test the strain could be calculated using the equation below. Small variations of the lattice spacing d_{hkl} to be measured lead to small variations of the Bragg's angle θ. The strains were calculated using the expression:

$$\varepsilon = \frac{\Delta d_{hkl}}{d_{hkl}} = -\cot\theta \cdot \frac{\Delta\theta}{\theta} \approx -\frac{\Delta D}{D}$$

The measurement of the transverse strain was a bit more difficult than the longitudinal one because the diffracted signal as well as the strain amplitude was very weak in this case.

The stress-free reference diameter for the strain measurements was chosen in regions where the material could be assumed to be close to a "stress-free" state i.e.: well away from the fibres for the titanium phase, and at the fibre end for the SiC phase. However, and despite these precautions, it can not be assumed that this reference diameter is really stress free. As a consequence we will use the term "relative strain" to qualify our measurements in what follows. Reflections 101 and 110 of the hexagonal titanium phase were used for the calculation of relative strains. Table 2 compares the crystalline stiffness measured here from the response of the fibre free regions with the values which can be calculated as suggested by Hill [10] (see Table 2). The table shows that our measurements are very close to the theoretical values.

In what follows, only the results obtained with reflection 110 of the titanium will be presented for reasons of brevity, but those obtained with reflection 101 are consistent. For the SiC, the only usable reflection was reflection 110. Figure 6 shows a profile of the longitudinal relative strain in the SiC and in the titanium around fibre 1 (a) and fibre 3 (b). Note that fibre 3 was broken before beginning the tensile test. Figure 7 shows the profile for the transverse relative strain around fibre 1 in the titanium (a) and in the SiC (b). These examples were chosen as very representative of the different observations made during the measurements.

Qualitatively the variations of the longitudinal relative strain can be described as follows. Before the tensile test, the matrix is slightly in tension around

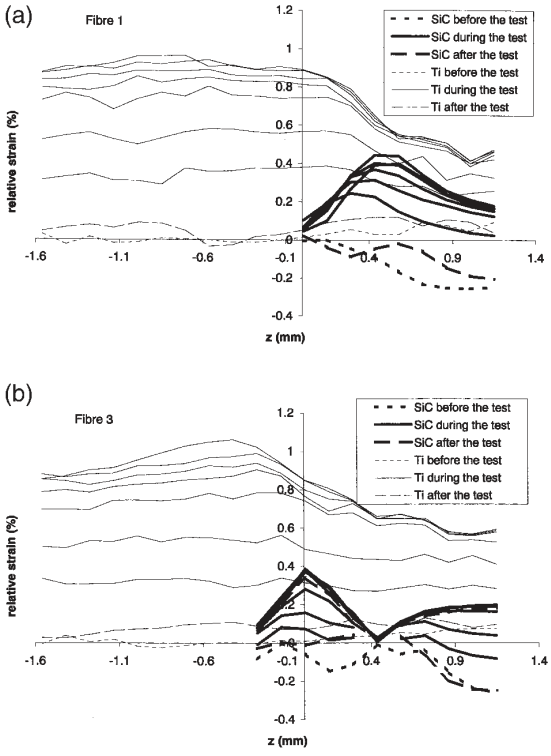

Fig. 6. The variation in the longitudinal strains measured during the tensile test along lines containing (a) fibre 1 and (b) fibre 3.

Table 2. Stiffness (all in GPa) measured for eachTi reflection and compared with the diffraction elastic constants (calculated as the mean of the bulk and single crystal values)

Reflection	Single crystal stiffness	Bulk	Diff E Constants	Experiment
{101}	142	115	128	126
{110}	103	115	109	107

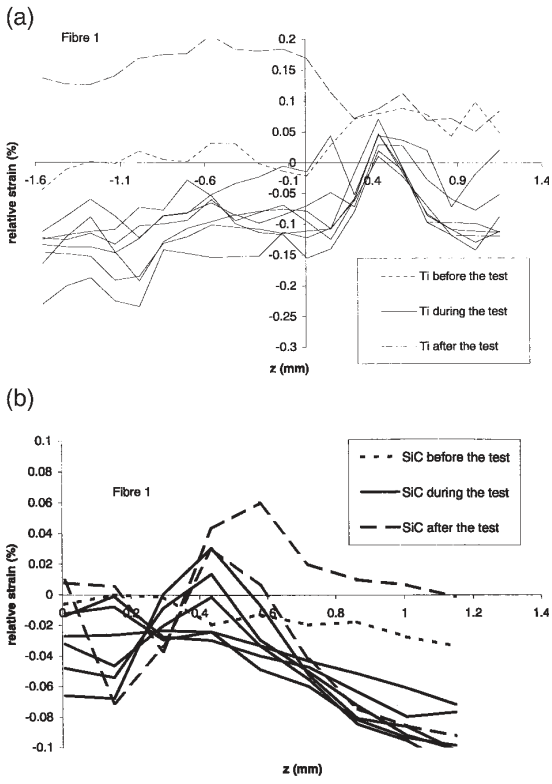

Fig. 7. Profiles of the transverse strains measured during the tensile test measured along a line including fibre 1 for (a) the Ti alloy and (b) for the SiC fibre 1.

the fibres and conversely the fibres are in compression. This is due to the thermal expansion misfit stresses generated by cooling from the hot pressing temperature. Note that the state of compression builds up from the fibre end, as one might expect from shear-lag type arguments [1]. Ahead of the fibres, the matrix is relatively unstressed. Because the incident beam samples a relatively small grain set, different families of grains will record slightly different strains due to intergranular effects. During elastic straining of the test-piece, the tensile component increases linearly in both fibre and matrix. There is a reduction in the relative strain of the matrix in the vicinity of the fibres due to the constraint they impose and the resulting load transfer in this region. On top of this a further reduction, which is seen in both fibres and matrix at a value of z of around 0.7 mm, is due to the influence of the shoulder of the sample which significantly increases the cross-section lowering the observed stresses. Throughout loading the fibre ends are essentially unstressed and there is a peak in the stress at a distance of about 0.5 mm from the ends. Given the resolution in the strain measurement and the size of the incident beam along the z direction the stress modifications caused by the fibre breakages in the immediate vicinity of the fibre ends could not be detected. The peak stress in the fibre appears to move away from the fibre end with increasing load although the effect of the test-piece shoulders should not be discounted. With plastic flow the elastic matrix strains soon begin to saturate, indicating a poor degree of strain hardening in the material which can also be seen on the global behaviour of the sample. The strains measured in fibre 7 were found to be very small which is consistent with the fact that this fibre was cut by the free surface and so was not completely embedded in the matrix. The axial residual strains are relatively small. The residual strains in the fibre-free region are due to the generation of intergranular stresses (plastic anisotropy) [11]. The residual strains in fibre 1 indicate that some of the initial residual strain has been washed out. This is presumably by sliding of the fibre under the tensile load.

Quantitatively the results are also satisfying. Taking into account the large original residual strain in the fibre, the change in strain during the test is from residual compression (-2000 microstrain) to applied tension (3000–4000 microstrain at the peak position) in the fibre. This corresponds to a change in strain of around 5000–6000 microstrains which compares relatively favourably with the change in microstrain in the matrix in the same region (i.e. from around $+600$ to around 5800 microstrain between unloaded and loaded which is equal to 5200 microstrain. This is less than the matrix only region because it contains around 7 vol% of fibres and so is approximately 20% stiffer. In fact the strains are in the ratio 6200:5200 microstrain between reinforced and unreinforced regions which represents 20% less strain (i.e. consistent with the stiffening of the reinforced region). The variation in the transverse strains in the fibre free region is consistent with a Poisson's ratio of 0.3. The tensile peak in transverse strain was unexpected and occurs approximately 0.4 mm from the fibre end (3 fibre diameters).

5. DISCUSSION

The amount of information given by the two parallel experiments presented in the preceding sections is very important. In order to understand better these observations, we have used a very simple finite element model to assess the values of the strains that could be reached in such a system. This calculation and its results are described in this section. They are then used as a basis to discuss the experimental observations.

5.1. FE modelling

An axi-symmetric model of the sample with only one fibre has been produced (see Fig. 8). Although the model does not describe completely the geometry of the problem, it was chosen as a compromise between model complexity/computation time and realism. The figure also shows the difference in geometry between the model used and the actual case studied. This difference lies mainly in the description of the interactions between the fibres. The deformation of this model has been studied using the

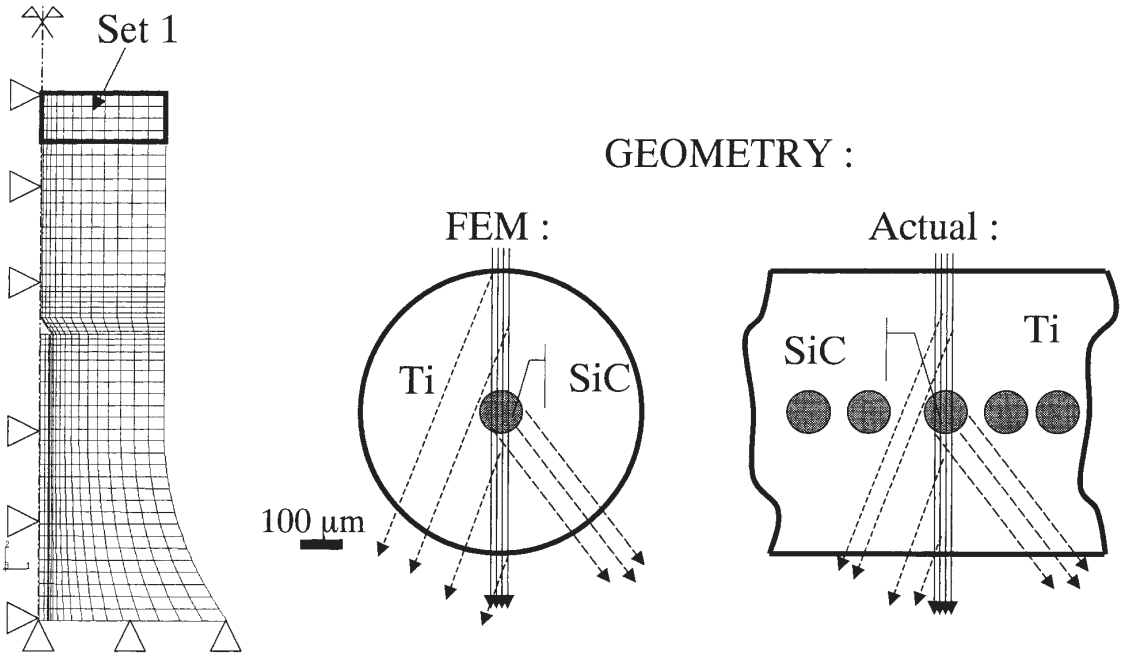

Fig. 8. Axi-symmetric mesh used for the FE element modelling of the sample. The bold rectangle shows one of the sets of elements used to average the strain in the calculations. Each set corresponds roughly to the gauge volume sampled during the diffraction experiment. The figure also shows the geometry assumed during the calculation and that used in the actual experiment.

ABAQUS code at stress levels corresponding to three of the first five steps of the actual tensile test (for stresses equal to 0, 584, and 900 MPa respectively). The bulk thermo-elastic properties for each phase were assumed to be isotropic and were taken for Ti as $E = 115$ GPa, $\nu = 0.36$ and $\alpha = 12\ 10^{-6}\ \mathrm{K}^{-1}$ and for SiC as $E = 415$ GPa, $\nu = 0.15$ and $\alpha = 4.8\ 10^{-6}\ \mathrm{K}^{-1}$. The plastic behaviour of the unreinforced matrix used was that measured by Withers and Clarke [11]. In the last step, the matrix was beginning to plastically deform. The bonding between fibre and matrix was assumed to be perfect (an over estimate of the shear stress between matrix and fibre which will be reduced in practice by frictional sliding) and the influence of the debris seen in the actual microstructure was neglected. However we did account for the presence of the pores which can be seen at the fibre ends by radiography.

The following results are presented in a form directly comparable to the experimental measurement which, despite the fine spatial resolution achieved in the present case, exhibit a certain degree of volume averaging. The calculated stress/strain values have been averaged over a set of elements corresponding roughly to the gauge volume sampled during the acquisition of one diffraction pattern (see Fig. 8). Figure 9 compares the results of the calculation for the titanium phase with these obtained around fibre 1 for both (a) the longitudinal and (b) the transverse components. Figure 10(a and b) show the same results for the SiC phase.

The samples were about 1 mm thick in the trans-

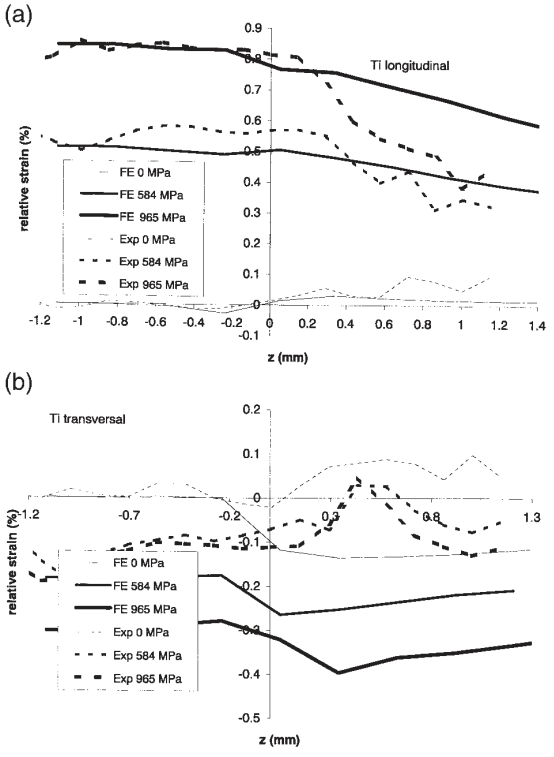

Fig. 9. (a) Axial and (b) transverse strains calculated using the FE model compared with the experimental results for the Ti matrix in the vicinity of fibre number 1.

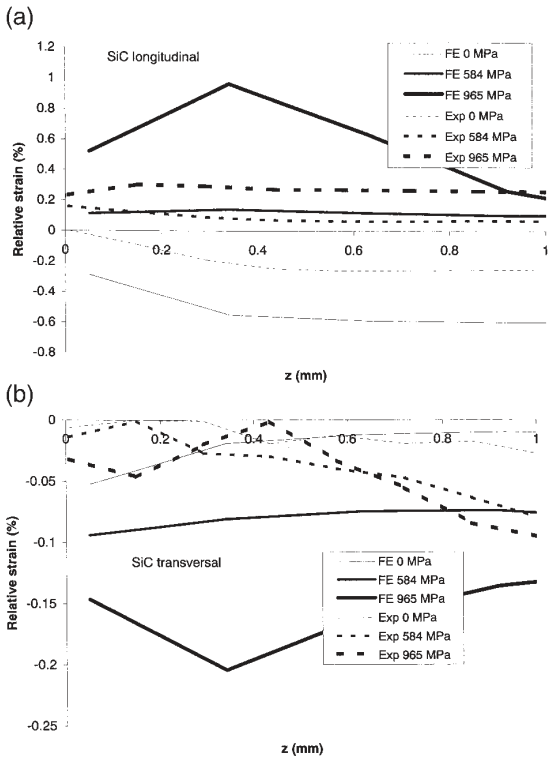

Fig. 10. (a) Axial and (b) transverse strains calculated with the FE model compared with the experimental results for the SiC fibre number 1.

mission direction so the SiC diffracting volume at each measurement location was approximately 10 times less than that of titanium. It should then be noted that the strain recorded for the titanium is an average over regions which are close and those at a greater radius from the nearest fibre (see Fig. 8).

In general, the evolution of the calculated value of the relative longitudinal strain agrees well with the measurements. The cooling of the sample has given rise to tensile strains in the matrix and compressive strains in the fibres. Not surprisingly, the strain increases in both phases with increased tensile loading of the sample. There is a kind of broad peak in the SiC strain and a drop in the matrix strain due to the combined effects of the specimen shoulder (which begins at around $z = 0.7$ mm) and load transfer from matrix to fibres.

Overall the calculated and measured longitudinal strain levels agree very well for the matrix. However, the strain reduction measured in the shoulder in the plastic regime is slightly less marked in the calculation. This might be due to a slight difference between the radius of the shoulder of the actual sample and that of the model.

As far as the prediction for the SiC is concerned, the model predicts that high plastic strains are induced in the matrix close to the fibre end. As a result of this combined with perfect matrix fibre bonding, the strain values predicted for the SiC are very large; much larger than those actually measured. This indicates a certain degree of sliding of the fibres during the straining in the actual case compared to the simple model used here. In other words, in the actual composite, the interface is certainly not perfectly bonded as the model assumes. This is not totally surprising given that the SCS6 fibres include a 4 μm carbon coating which is likely to encourage sliding. Further FEM calculations with sliding interfaces are currently being carried out to check this point.

The qualitative and quantitative predictions of the transverse strain, due to Poisson's effects, are less well matched to the data. For the titanium, the transverse strain is larger in the calculation away from the fibres. Moreover the qualitative evolution is not very well represented close to the fibres. This could be due either to the lower precision of the strain measurements in the transverse direction, but also to the difference between the model (one single fibre) and the actual geometry (several adjacent interacting fibres). Since the influence of the region close to the SiC should be minor on the titanium diffraction signal, the precision of the measurement might be the explanation.

For the SiC, the strain evolution is well described qualitatively, but the measured variation in strain is much smaller than the prediction which could also be due to the sliding at the interface. There could also be here an effect of the neighbouring fibres that could reduce the transverse deformation in the experimental case.

6. CONCLUSIONS

The current study into the evolution of strain and damage in the individual fibres of a composite testpiece demonstrates the power of combining radiography and high spatial resolution diffraction strain measurement. The latter provides the information about the internal strain distribution, while the former provides information about the effects of these stresses on damage accumulation through micromechanisms such as matrix voiding, interface sliding and fibre breakage.

The important findings are as follows:

1. Fibre breakages did not occur evenly as the load was increased, rather breakages were clustered in space and time (load).
2. Initial thermal residual strains were observed in the fibres (axial compression) and neighbouring matrix (tension).
3. At a given load the fibre strains built up from the fibre ends; the level of straining increased as the load increased.
4. Perhaps surprisingly a number of fibre breakages occurred near the fibre ends (within a few fibre diameters). This was unexpected and was not

coincident with the region of largest elastic fibre strain.

5. Guillotining the fibres in the manufacturing process clearly damaged the fibre ends and this may be responsible for the occurrences of further cracking in this region with increased loading. The hot pressing stage had introduced cavities at each fibre end.
6. The fibre stress distribution within the fragmented section of Fibre 3 was triangular in form similar to the results obtained by other methods on polymeric composites [3]. The build-up of stress is believed to be controlled by the interface sliding in the carbon interlayer between the SiC monofilaments and the Ti–6Al–4V matrix. Further modelling work is required to simulate the build-up of stress in this segment and thus to examine whether the stress distribution is consistent with previous measures of the interfacial shear behaviour made using other techniques.
7. A simple FE model was useful for the interpretation of the axial strain measurements but could not mimic the transverse behaviour.

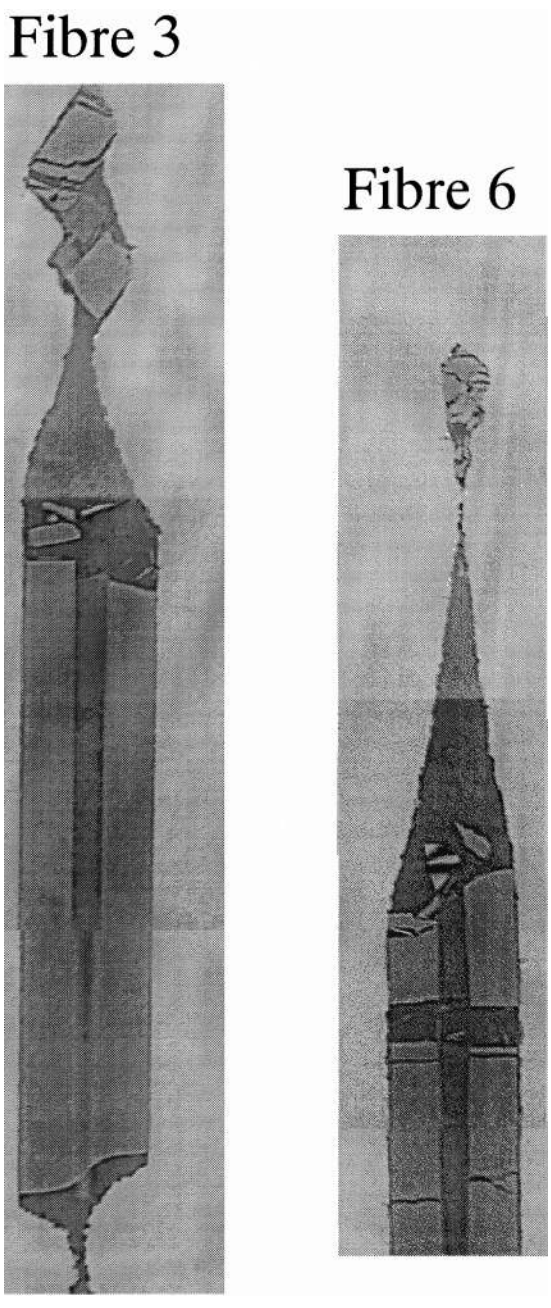

Fig. 11. Tomographic slices taken from the reconstructed volume of sample 2 measured after testing.

In the present monolayer case simple radiographs have been sufficient to study the behaviour of the fibre ends and the onset of fibre breakage with a resolution of 6 μm using attenuation contrast. Phase contrast around fibre breakages highlight the onset of cracks even when they are much smaller than this. The final tomographs (Fig. 11) show the much greater level of detail that can be obtained by the acquisition of full tomographs. From these the 3D nature of the debris and fibre cracking can be unequivocally deduced. Furthermore, recent improvements in the set-up at ID19 have lead to an improvement in the spatial resolution achievable to 1 μm and a shortening of the time required to collect complete tomographs to under 15 min.

At the present time there is no beam-line tailored to the simultaneous or sequential acquisition of radiographic images and strain maps. Future work will see the transfer of a single sample between the ID19 and ID11 beam lines to study damage and strain evolution on a single sample.

Acknowledgements—Wolfgang Ludwig and Laurent Babout were of great help during the radiography experiment on ID19. The authors wish also to acknowledge Ann Terry, Gavin Vaughan, Judy Pang and Mark Pinkerton for help on the ID11 part of the experiment and Alex Madgwick for fabricating the test-samples. An Alliance/British Council grant to facilitate travel between France and England is gratefully acknowledged. The beam-time at the ESRF was made available through the normal academic peer reviewed access route.

REFERENCES

1. Clyne, T. W. and Withers, P. J., *An Introduction to Metal Matrix Composites*, Cambridge Solid State Series. Cambridge University Press, Cambridge, 1993.
2. Schadler, L. S. and Galiotis, C., *Int. Mater. Rev.*, 1995, **40**, 116.
3. Huang, Y. and Young, R. J., *Comp. Sci. Technol.*, 1994, **52**, 505.
4. Kieschke, R. R. and Clyne, T. W., in *Interfacial Phenomena in Composite Materials*., Butterworths, Oxford, 1989.
5. Yang, C. J., Jeng, S. M. and Yang, J. M., *Scripta Metall. Mater.*, 1990, **24**, 469.
6. Le Petitcorps, Y., Pailler, R. and Naslain, R., *Comp. Sci. Technol.*, 1989, **35**, 207.
7. Watson, M. C. and Clyne, T. W., *Acta Metall. Mater.*, 1992, **40**, 141.
8. Cloetens, P., Pateyron-Salomé, M., Buffière, J. Y., Peix, G., Baruchel, J., Peyrin, F. and Schlenker, J., *J. Appl. Phys.*, 1997, **81**, 9.

9. Buffière, J. -Y., Maire, E., Cloetens, P., Lormand, G. and Fougères, R., *Acta Metall.*, 1999, **47**(5), 1613.
10. Hill, R., *Proc. Phys. Soc. Lond.*, 1952, **A65**, 349.
11. Withers, P. J. and Clarke, A. P., *Acta Mater.*, 1998, **46**, 6585.